




## Article

# A Novel Bio-Inspired Ag/3D-TiO<sub>2</sub>/Si SERS Substrate with Ordered Moth-like Structure

Jingguo Yang <sup>1,†</sup>, Florian Ion Tiberiu Petrescu <sup>2,†</sup> , Ying Li <sup>1</sup>, Dandan Song <sup>1</sup> and Gang Shi <sup>1,\*</sup>

<sup>1</sup> Key Laboratory of Synthetic and Biotechnology Colloids, Ministry of Education, School of Chemical and Material Engineering, Jiangnan University, Wuxi 214122, China

<sup>2</sup> Department of Mechanisms and Robots Theory, Bucharest Polytechnic University, 060042 Bucharest, Romania

\* Correspondence: gangshi@jiangnan.edu.cn or shigang0720@126.com

† These authors contributed equally to this work.

**Abstract:** This paper reports a novel method to fabricate a bio-inspired SERS substrate with low reflectivity, ultra-sensitivity, excellent uniformity, and recyclability. First, double layers of polystyrene spheres with different particle sizes were assembled on the surface of a silicon wafer to act as a moth-like template. Second, through the template sacrifice method, the TiO<sub>2</sub> film with a three-dimensional moth-like eye structure was induced by the double-layer polystyrene spheres in the previous step, and its microscopic morphology showed a high degree of order. Finally, Ag nanoparticles were assembled on the TiO<sub>2</sub> film to form a bio-inspired SERS substrate. This ordered bio-inspired structure can not only reduce reflection, but also reinforce the uniformity of hotspot density, which helps to improve the sensitivity and uniformity of the Raman signal. This bio-inspired SERS substrate can detect R6G molecules at a concentration as low as  $1.0 \times 10^{-10}$  mol/L, and its enhancement factor (EF) can reach  $6.56 \times 10^6$ . In addition, the composite of Ag and TiO<sub>2</sub> can realize the photocatalytic degradation of R6G and then realize the recyclability of the SERS substrate.



**Citation:** Yang, J.; Petrescu, F.I.T.; Li, Y.; Song, D.; Shi, G. A Novel Bio-Inspired Ag/3D-TiO<sub>2</sub>/Si SERS Substrate with Ordered Moth-like Structure. *Nanomaterials* **2022**, *12*, 3127. <https://doi.org/10.3390/nano12183127>

Academic Editor: Isabel Pastoriza-Santos

Received: 2 August 2022

Accepted: 6 September 2022

Published: 9 September 2022

**Publisher's Note:** MDPI stays neutral with regard to jurisdictional claims in published maps and institutional affiliations.



**Copyright:** © 2022 by the authors. Licensee MDPI, Basel, Switzerland. This article is an open access article distributed under the terms and conditions of the Creative Commons Attribution (CC BY) license (<https://creativecommons.org/licenses/by/4.0/>).

**Keywords:** SERS; bio-inspired; ultra-sensitivity; recyclability

## 1. Introduction

Surface-enhanced Raman scattering (SERS) is an important method for the analysis of trace substances, which has been widely applied to the detection of chemical substances, biomolecules, and environmental pollutants [1–5]. It has the advantages of excellent specificity and high sensitivity to the target analytes [6–8]. Generally, the Raman signal enhancement is usually attributed to the electromagnetic field effect [9–11] of the substrate, and the noble metals on it play a leading role [12–14]. The surface microstructure of the SERS substrate has a great impact on the Raman signal intensity, and the three-dimensional (3D) structure usually has the stronger Raman signal [15–17]. On the one hand, the 3D structure can provide more effective hotspots [18,19]. On the other hand, the 3D structure with a high specific surface area can adsorb more target analytes, thus improving the Raman signal. Furthermore, the 3D structure has excellent antireflective performance, which can increase the absorption efficiency of excited light, and then improve the Raman signal [20,21].

Most SERS substrates can only be used once because the analytes adsorbed on the surface of the SERS substrate are not easily removed. Therefore, current research usually focuses on the development of recyclable SERS substrates [22–24]. TiO<sub>2</sub> is an excellent photocatalytic material, of which composites with noble metals (such as Au, Ag, Cu, etc.) not only improve the photocatalytic efficiency, but also expand the SERS capability. This noble metal/TiO<sub>2</sub> composite can achieve the recyclability of the SERS substrate [25–27]. In addition to recyclability, the uniformity of the Raman signal is one of the important evaluation factors for SERS substrates. Fabricating an ordered micro/nano-structure is an effective way to achieve the uniformity of the Raman signal. The ordered micro/nano-structure

(such as spheres, rods, bowls, etc.) of  $\text{TiO}_2$  and its composite substrates can be obtained by the sol-gel method, hydrothermal method, and chemical vapor deposition [28–30]. Among them, the metal film-covered ordered  $\text{TiO}_2$  sphere (MOTS) SERS substrate has always been focused on due to its stability, uniformity, and recyclability. However, the traditional MOTS SERS substrate still needs improvement to enhance the detection sensitivity.

The antireflective ability of moth-eye structures can effectively improve the absorption efficiency of incident light, so it is worth considering how to apply this to the MOTS substrate to enhance the Raman signal intensity. Here, a two-step colloidal spheres template method is proposed to fabricate a  $\text{Ag}/3\text{D-TiO}_2/\text{Si}$  composite SERS substrate with an ordered moth-like eye structure. This SERS substrate can not only improve the intensity and uniformity of Raman signal at the same time, but also realize the recyclability of the substrate. The SERS substrate contains noble metal Au or Ag, which have high costs. In the detection process, organic molecules adsorbed on the traditional SERS substrate are difficult to remove, which will have a non-negligible impact on the subsequent detection. Therefore, it can only be used once, which limits the promotion and application to families, such as the detection of drinking water, fruits, vegetables, milk, meat, and so on. Based on the consideration of the above problems, this study developed a reusable SERS substrate to reduce its use cost, which provided the possibility of applying the SERS base to home detection.

## 2. Materials and Methods

### 2.1. Chemicals and Materials

Acetone ( $\text{CH}_3\text{COCH}_3$ ), chloroform ( $\text{CHCl}_3$ ), ethanol ( $\text{CH}_3\text{CH}_2\text{OH}$ ), hydrochloric acid ( $\text{HCl}$ ), n-butyl titanate ( $\text{C}_{16}\text{H}_{36}\text{O}_4\text{Ti}$ ), stannous chloride dihydrate ( $\text{SnCl}_2 \cdot 2\text{H}_2\text{O}$ ), sodium dodecyl sulfate (SDS), rhodamine 6G (R6G), and potassium persulfate (KPS) were purchased from Sinopharm Chemical Reagent Co., LTD., Shanghai, China. Silver nitrate ( $\text{AgNO}_3$ ) and styrene ( $\text{C}_8\text{H}_8$ ) were purchased from Sigma Aldrich Trading Co., LTD., St. Louis, MO, USA. All reagents were used directly without further purification. The Si wafers (p-type (100)) were obtained from Youyan Guigu, Beijing, China. Distilled water was used.

### 2.2. Fabrication of 2D and 3D Polystyrene (PS) Templates

PS spheres with different particle sizes (1570 nm and 180 nm) were synthesized by the emulsion polymerization method [31–33]. Then, the 2D and 3D PS templates were fabricated by the self-assembly method, and the detailed procedures are as follows.

Firstly, 10 wt% 1570 nm of PS spheres suspension was diluted with the same amount of ethanol and then dropped onto the water surface. Secondly, a drop of 5% SDS was added to form a closely packed monolayer of PS spheres, and then it was assembled on the Si wafer. Thirdly, the solvent was evaporated to obtain the 2D PS template. After heating at  $90^\circ\text{C}$  for 5 min, the adhesion between PS microspheres and the substrate was increased. Fourthly, 180 nm of PS spheres were continued to assemble on the above 2D PS template in accordance with the above method. Finally, the 3D PS template was received after drying under natural conditions.

### 2.3. Fabrication of 2D- $\text{TiO}_2/\text{Si}$ and 3D- $\text{TiO}_2/\text{Si}$

$\text{TiO}_2$  sol was obtained by classical hydrolysis of n-butyl titanate and diluted to 0.213 mol/L [34]. Then, 30  $\mu\text{L}$  of  $\text{TiO}_2$  sol was spin-coated onto the 2D or 3D colloidal template. The above samples were placed in a muffle furnace at  $450^\circ\text{C}$  for 2 h with a heating rate of  $1^\circ\text{C}/\text{min}$ . When  $\text{TiO}_2$  was coated on the 2D PS template and calcined, the obtained sample was named 2D- $\text{TiO}_2/\text{Si}$ . When  $\text{TiO}_2$  was coated on the 3D PS template and calcined, the obtained sample was named 3D- $\text{TiO}_2/\text{Si}$ .

### 2.4. Fabrication of $\text{Ag}/2\text{D-TiO}_2/\text{Si}$ and $\text{Ag}/3\text{D-TiO}_2/\text{Si}$

After 0.1 mol/L  $\text{SnCl}_2$  solution was mixed with 0.02 mol/L  $\text{AgNO}_3$  solution, 2D- $\text{TiO}_2/\text{Si}$  or 3D- $\text{TiO}_2/\text{Si}$  were immediately immersed in the mixed solutions and reacted at

60 °C for 8 h. Thus, a certain amount of Ag NPs was deposited on the TiO<sub>2</sub> surface [35]. The SERS substrates after Ag deposition on 2D-TiO<sub>2</sub>/Si and 3D-TiO<sub>2</sub>/Si were named Ag/2D-TiO<sub>2</sub>/Si and Ag/3D-TiO<sub>2</sub>/Si, respectively. From the experimental preparation to the successful fabrication of Ag/3D-TiO<sub>2</sub>/Si, the whole process took 29 h. The sample area can be up to 4 cm × 4 cm.

### 2.5. Raman Measurements

The substrates were immersed in R6G ethanol solution for 30 min and then washed with deionized water. The Raman spectrum was measured immediately after the above substrates were dried with nitrogen.

### 2.6. Photocatalytic Measurements

The photocatalytic capability of the substrates (1.0 cm × 2.0 cm) was measured by the degradation of R6G under irradiation of the 300 W Xe light source (200 nm < λ < 2500 nm). The substrates were immersed in 2 mL of the R6G solution (10<sup>−4</sup> mol/L, neutral condition) and stirred in the dark for 30 min to ensure adsorption equilibrium before the illumination. After the illumination, the R6G solution was immediately measured using a UV-vis spectrophotometer.

### 2.7. Photoelectrochemical (PEC) Measurements

The photocurrent intensity and the electrochemical impedance evaluations were measured in a standard three-electrode system [36,37]. PEC measurements were performed with the substrates, Pt filament, and Ag/AgCl as the working electrode, the counter electrode, and the reference electrode, respectively. The PEC capability was measured by the electrochemical analyzer with 0.5 mol/L Na<sub>2</sub>SO<sub>4</sub> solution as the electrolyte, and the simulated solar light source (100 mW/cm<sup>2</sup>) was irradiated in the 1.0 × 1.0 cm<sup>2</sup> area from the front of the working electrode.

### 2.8. Characterizations

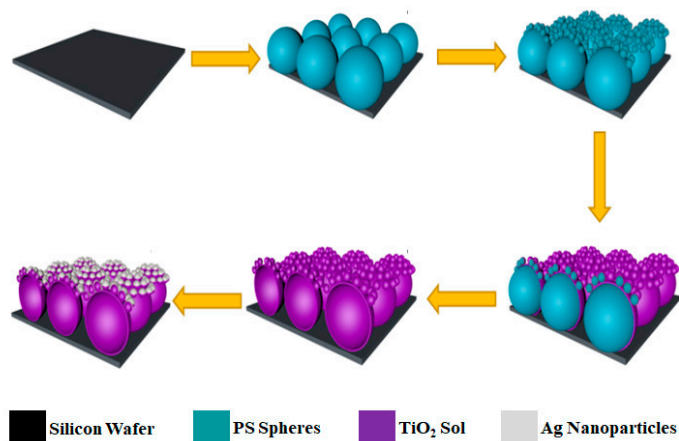
SEM was performed using a Hitachi S4800 (Hitachi, Tokyo, Japan) microscope. UV-vis spectra were recorded using a UV-vis spectrometer (UV-3600 plus, Shimadzu, Kyoto, Japan). The photocurrent response and the resistance effect were recorded by an electrochemical station (CHI-660, Shanghai Chenhua, Shanghai, China). Photocatalytic degradation was carried out under a 300 W xenon lamp (CEL-HXF 300, CEAuLight Co., Ltd., Beijing, China) as the visible light source. The Raman spectra were recorded at room temperature on a Raman system (Renishaw inVia, Renishaw plc, Gloucestershire, UK) equipped with a charge-coupled device (CCD) detector and a 532 nm laser of 0.05 mW. The spot diameter of the laser was 2 μm. Signal accumulation with an integration time of 10 s was used to collect the spectra for all Raman measurements.

## 3. Results and Discussion

### 3.1. Fabrication and Surface Characterization of SERS Substrate

The fabrication process of the Ag/3D-TiO<sub>2</sub>/Si substrate with a 3D moth-like eye structure is shown in Scheme 1. First, monolayers of PS spheres with diameters of 1570 nm and 180 nm were assembled on the Si wafer successively by the interfacial assembly and transfer technique. Figure 1a,b are the SEM images of 1570 nm monolayer PS spheres, which are uniform in size, compact in arrangement, and highly ordered in a large area. Second, 180 nm PS spheres were assembled on the surface of 1570 nm PS spheres through a similar method described above. Figure 1c,d show that each 1570 nm PS sphere is covered with 30–50 of 180 nm PS spheres. This two-size hierarchical structure imitates the moth-eye structure, which was used as a template to fabricate the bio-inspired SERS substrate. Third, the TiO<sub>2</sub> sol was coated on the surface of the above template, and the PS spheres were then removed by high-temperature calcination to obtain the TiO<sub>2</sub> film with an ordered moth-like eye structure, as shown in Figure 1e,f. The calcined TiO<sub>2</sub> is in anatase form, as shown in

Figure S1. Finally, Ag NPs were deposited on  $\text{TiO}_2$  by the in situ reduction method of  $\text{Sn}^{2+}$ , and the obtained sample is referred to as Ag/3D- $\text{TiO}_2$ /Si. Ag NPs with a particle size of 20–60 nm are densely packed around the porous  $\text{TiO}_2$ , as shown in Figure 1g,h. Through the EDS characterization of Ag/3D- $\text{TiO}_2$ /Si (Figure 2), it is further proved that the bio-inspired SERS substrate has been fabricated successfully.



**Scheme 1.** Scheme of fabricating the Ag/3D- $\text{TiO}_2$ /Si substrate with 3D moth-like eye structure.

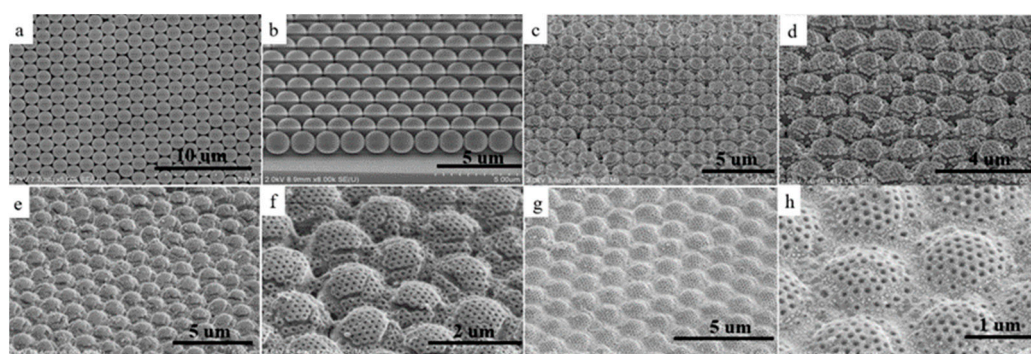


**Figure 1.** SEM images of the substrates. (a,b) 2D PS template; (c,d) 3D PS template; (e,f) 3D- $\text{TiO}_2$ /Si; (g,h) Ag/3D- $\text{TiO}_2$ /Si.

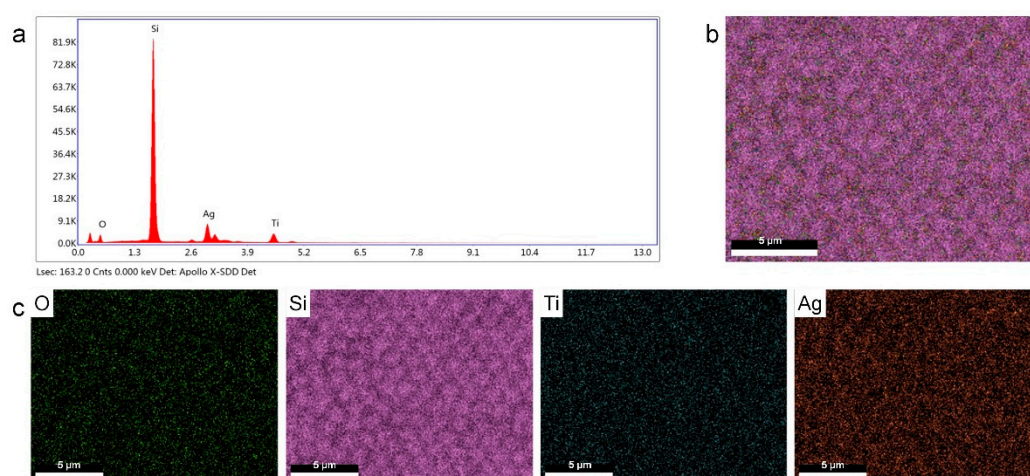


**Figure 2.** (a) EDS spectrum of Ag/3D- $\text{TiO}_2$ /Si; (b) EDS element mapping image of Ag/3D- $\text{TiO}_2$ /Si; (c) EDS mapping images of elements O, Si, Ti, and Ag.



### 3.2. Raman Performance of Ag/3D-TiO<sub>2</sub>/Si

It can be seen from Figure 3a that the Raman signal of R6G adsorbed on the Ag/3D-TiO<sub>2</sub>/Si substrate is significantly stronger than that of others, which is mainly attributed to the following two aspects. First, the 3D structure of Ag/3D-TiO<sub>2</sub>/Si increases the number of hotspots compared with the 2D structure of Ag/2D-TiO<sub>2</sub>/Si. According to the SEM images of Ag/3D-TiO<sub>2</sub>/Si (Figure 1g,h) and Ag/2D-TiO<sub>2</sub>/Si (Figure S2), the former substrate has a larger number of regular porous structures than the latter. As a result, the specific surface area is larger, and the loaded Ag NPs are relatively more abundant; thus, Ag/3D-TiO<sub>2</sub>/Si will create more hotspots and more adsorption sites, which is conducive to the enhancement of the Raman signal. Second, the 3D moth-like eye structure of Ag/3D-TiO<sub>2</sub>/Si conforms to the equivalent medium theory [36,38–41], which will make the refractive index change gradually from the air to the substrate, and then the incident light reflection will be reduced; in other words, the incident light absorption will be enhanced. Therefore, the reflectivity of Ag/3D-TiO<sub>2</sub>/Si is significantly lower than that of Ag/2D-TiO<sub>2</sub>/Si, as shown in Figure 3b, which is conducive to the enhancement of the Raman signal. It is worth noting that Ag/3D-TiO<sub>2</sub>/Si has a wide wavelength absorption band at 400–600 nm, which is attributed to the plasmon resonance absorption [42–44] on the substrate surface, which is beneficial to the enhancement of the Raman signal [45].

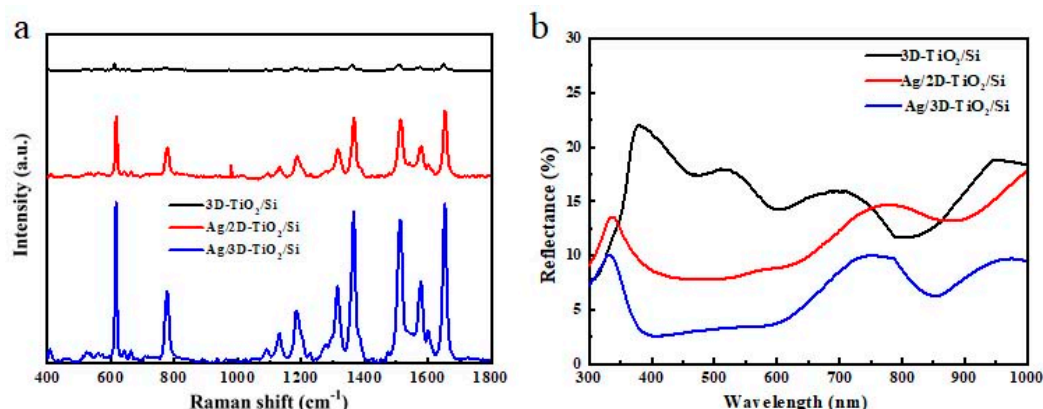


**Figure 3.** (a) Raman spectra of R6G on the different substrates; (b) reflectance spectra of the different substrates.

The detection sensitivity is also an important property in evaluating the performance of the SERS substrate. Here, the Ag/3D-TiO<sub>2</sub>/Si substrates were immersed in different concentrations of R6G ethanol solutions, and their corresponding Raman spectra are shown in Figure 4a. With the decrease in R6G concentration, the Raman signals are gradually decreased. The concentration of R6G detected by the SERS substrate is as low as 10<sup>−10</sup> mol/L. This indicates that the Ag/3D-TiO<sub>2</sub>/Si substrate has high sensitivity. In addition, the uniformity of the SERS substrate is also an important property. Figure 4b shows the Raman spectra of R6G (10<sup>−4</sup> mol/L) at 20 random points of the Ag/3D-TiO<sub>2</sub>/Si substrate. The relative standard deviation (RSD) of the Raman characteristic peak at 1368 cm<sup>−1</sup> is 9.0%, implying that Ag/3D-TiO<sub>2</sub>/Si has excellent uniformity. This is because the 3D structure of the Ag/3D-TiO<sub>2</sub>/Si substrate is highly ordered, and the Ag NPs are evenly distributed.

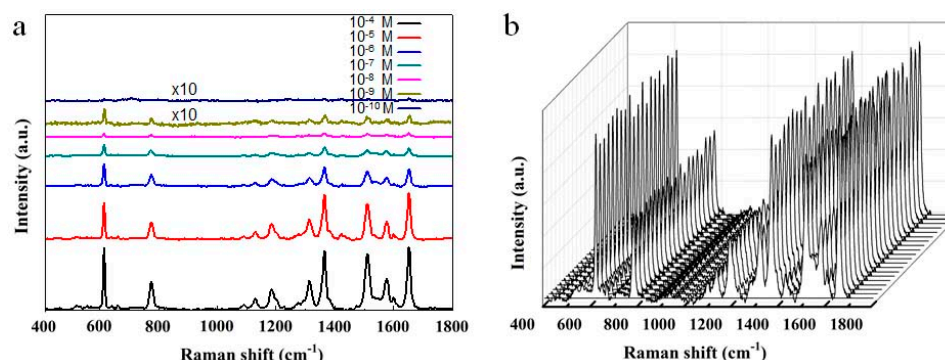


**Figure 4.** (a) Raman spectra of R6G with the concentrations of  $10^{-4}$ ,  $10^{-5}$ ,  $10^{-6}$ ,  $10^{-7}$ ,  $10^{-8}$ ,  $10^{-9}$ , and  $10^{-10}$  mol/L on the Ag/3D-TiO<sub>2</sub>/Si substrate. (The signal is expanded 10 times at the R6G concentration of  $10^{-9}$  and  $10^{-10}$  mol/L.); (b) Raman spectra of R6G with the concentration of  $10^{-4}$  mol/L adsorbed at 20 random points of the Ag/3D-TiO<sub>2</sub>/Si substrate.

The enhancement factor ( $EF$ ) is an important parameter to evaluate the Raman enhancement of the SERS substrates, and the specific formula is as follows [33,46]:

$$EF = \frac{I_{\text{SERS}} \times N_0}{N_{\text{SERS}} \times I_0} \quad (1)$$

where  $I_{\text{SERS}}$  and  $I_0$  are the Raman peak ( $1368 \text{ cm}^{-1}$ ) intensities of R6G on the Ag/3D-TiO<sub>2</sub>/Si substrate and the Si wafer, respectively.  $N_{\text{SERS}}$  and  $N_0$  are the number of R6G molecules on the Ag/3D-TiO<sub>2</sub>/Si substrate and the silicon wafer, respectively.

The R6G molecules on the substrate are considered to be distributed uniformly; thus,  $N_{\text{SERS}}$  and  $N_0$  can be estimated by the following formula:

$$N = \frac{N_A M V S_{\text{laser}}}{S_{\text{sub}}} \quad (2)$$

where  $N_A$  is Avogadro's constant,  $M$  is the concentration of the R6G solution,  $V$  is the volume of the droplet,  $S_{\text{sub}}$  is the substrate area ( $1 \text{ cm}^2$ ), and  $S_{\text{laser}}$  is the laser point area ( $1 \text{ }\mu\text{m}^2$ ). Here,  $10 \text{ }\mu\text{L}$  of  $10^{-8}$  mol/L R6G solution is dropped onto the Ag/3D-TiO<sub>2</sub>/Si substrate, while for the Si wafer,  $10 \text{ }\mu\text{L}$  of  $10^{-2}$  mol/L R6G solution is dropped onto it. Based on the peak intensity of  $1368 \text{ cm}^{-1}$  in the Raman spectra of Figure 5 and combined with Equations (1) and (2),  $EF = 6.56 \times 10^6$  is evaluated.

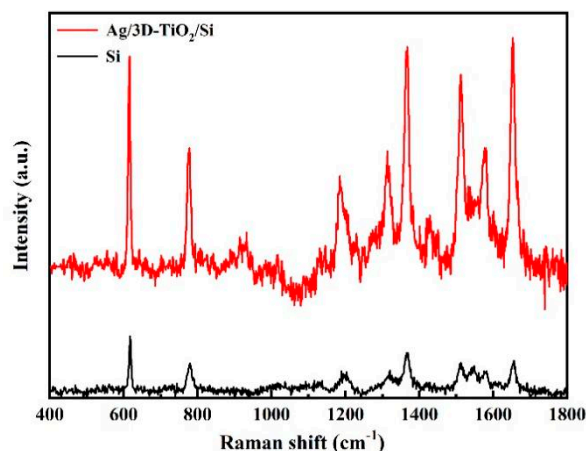


**Figure 5.** Raman spectra of  $10^{-2}$  mol/L R6G solution on the Si wafer and  $10^{-8}$  mol/L R6G solution on the Ag/3D-TiO<sub>2</sub>/Si substrate.

### 3.3. Photocatalysis and Recyclability of Ag/3D-TiO<sub>2</sub>/Si

According to the dark state adsorption test, the concentration of R6G is almost unchanged after adsorption–desorption equilibrium. Figure 6a shows the absorption spectra of R6G in the process of photocatalytic degradation by the Ag/3D-TiO<sub>2</sub>/Si substrate under simulated solar radiation. With the extension of time, the R6G concentration decreases gradually until it no longer changes after two hours. It can be found from Figure 6b that the Ag/3D-TiO<sub>2</sub>/Si substrate has the fastest catalytic degradation rate and the best photocatalytic capability on R6G. The excellent photocatalytic degradation of R6G by Ag/3D-TiO<sub>2</sub>/Si can ensure the self-cleaning of the SERS substrate so as to realize recyclable SERS detection. The Raman signal of the Ag/3D-TiO<sub>2</sub>/Si substrate was tested after the adsorption of R6G molecules with a concentration of 10<sup>−4</sup> mol/L (detection step). After the substrate was treated with the simulated solar irradiation for 2 h, the Raman signal almost completely disappeared (self-cleaning step). After four cycles of detection/self-cleaning, the Raman signal intensity of the substrate remained almost unchanged, corresponding to RSD (the Raman characteristic peak at 1368 cm<sup>−1</sup>) of 4.1%, as shown in Figure 6c. These results fully prove the excellent recyclability of the ordered 3D SERS substrate.

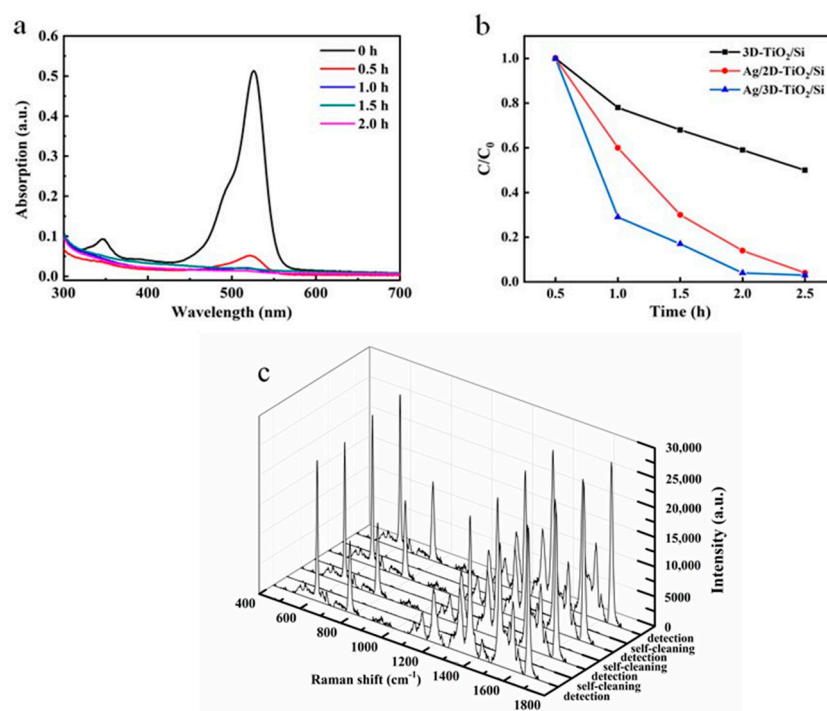


**Figure 6.** (a) UV-vis spectra of R6G under the simulated solar irradiation for different time by Ag/3D-TiO<sub>2</sub>/Si; (b) photocatalytic activity of different substrates for the degradation of R6G under the simulated solar irradiation; (c) the SERS spectra of Ag/3D-TiO<sub>2</sub>/Si at R6G concentrations of 10<sup>−4</sup> mol/L and the SERS spectra of the substrate treated with the simulated solar irradiation after adsorption of R6G.

In order to further analyze the reasons for the excellent photocatalytic performance of the Ag/3D-TiO<sub>2</sub>/Si substrate, linear sweep voltammograms (LSVs) and impedance characterization were performed, as shown in Figure 7a,b. In the dark, the photocurrent densities of Ag/3D-TiO<sub>2</sub>/Si, Ag/2D-TiO<sub>2</sub>/Si, and 3D-TiO<sub>2</sub>/Si are almost zero, and their corresponding curves are very similar. By comparing the Ag/3D-TiO<sub>2</sub>/Si substrate and the 3D-TiO<sub>2</sub>/Si substrate, the photocurrent density of the former is higher than that of the latter, and the internal resistance of the former is lower than that of the latter. This is because Ag NPs inhibit the photogenerated electron–hole pairs recombination of TiO<sub>2</sub>, which is conducive to the improvement in photocatalytic efficiency. In addition, by comparing the Ag/3D-TiO<sub>2</sub>/Si substrate and the Ag/2D-TiO<sub>2</sub>/Si substrate, the photocurrent density

of the former is higher than that of the latter, and the internal resistance of the former is lower than that of the latter. This is because the 3D moth-like eye structure has excellent antireflection performance, which is beneficial to improving the absorption efficiency of the incident light, thus increasing the number of TiO<sub>2</sub> photogenerated electron–hole pairs, and then the photocatalytic efficiency of the SERS substrate will be improved.

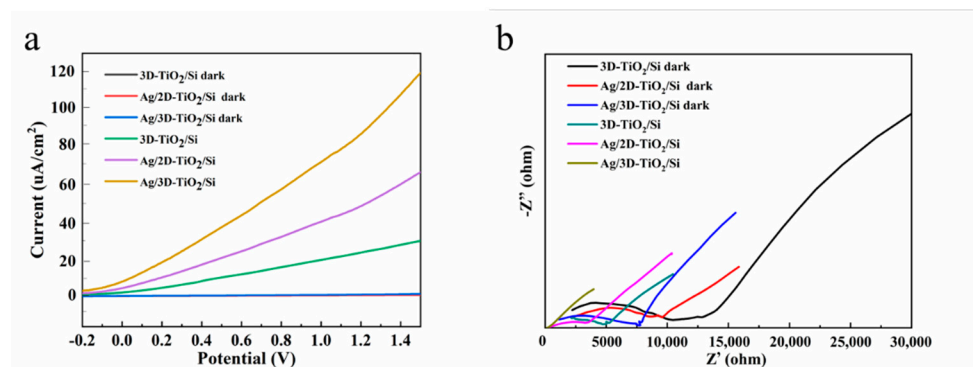


**Figure 7.** (a) LSV and (b) electrochemical impedance spectroscopy of different substrates.

#### 4. Conclusions

In summary, a 3D TiO<sub>2</sub> film with moth-like eye structure was fabricated on the Si wafer by the colloidal self-assembly method and then covered with a layer of uniformly distributed Ag NPs to form a novel SERS substrate. This bio-inspired structure not only reduced the reflection, but also provided more hotspots in the laser radiation area. R6G as low as  $1.0 \times 10^{-10}$  mol/L was still detected by the Ag/3D-TiO<sub>2</sub>/Si substrate, and the corresponding EF reached  $6.56 \times 10^6$ . The ordered structure of Ag/3D-TiO<sub>2</sub>/Si resulted in the uniformity of Raman signals (RSD = 9.0%). Meanwhile, the Ag/3D-TiO<sub>2</sub>/Si substrate was recyclable due to its excellent photocatalysis. This study developed a reusable SERS substrate to reduce its use cost, which provides the possibility of applying SERS base to home detection, such as the detection of drinking water, fruits, vegetables, milk, meat, and so on.

**Supplementary Materials:** The following supporting information can be downloaded at: <https://www.mdpi.com/article/10.3390/nano12183127/s1>, Figure S1: XRD of TiO<sub>2</sub> and TiO<sub>2</sub> deposited with Ag NPs; Figure S2: SEM images of (a) 2D-TiO<sub>2</sub>/Si and (b) Ag/2D-TiO<sub>2</sub>/Si.

**Author Contributions:** Conceptualization, G.S.; methodology, G.S.; validation, G.S.; formal analysis, J.Y. and F.I.T.P.; investigation, J.Y. and F.I.T.P.; resources, J.Y. and F.I.T.P.; data curation, Y.L. and D.S.; writing—original draft preparation, J.Y. and F.I.T.P.; writing—review and editing, Y.L. and D.S.; project administration, G.S.; funding acquisition, G.S. All authors have read and agreed to the published version of the manuscript.

**Funding:** This work was supported by National Natural Science Foundation of China (21671081), Science and Technology Support Program of Jiangsu Province (BE2020381), Fok Ying Tong Education Foundation (171039) and Tibetan Medicine “the 14th Five-Year Plan” Connotation Construction Project (2021ZYYGH003, 2021ZYYGH006, 2021ZYYGH007).

**Institutional Review Board Statement:** Not applicable.

**Informed Consent Statement:** Not applicable.

**Acknowledgments:** The support from Central Laboratory, School of Chemical and Material Engineering, Jiangnan University, is appreciated.

**Conflicts of Interest:** The authors declare no conflict of interest.



## References

1. Zeng, Y.; Ananth, R.; Dill, T.J.; Rodarte, A.; Rozin, M.J.; Bradshaw, N.; Brown, E.R.; Tao, A.R. Metasurface-Enhanced Raman Spectroscopy (mSERS) for Oriented Molecular Sensing. *ACS Appl. Mater. Interfaces* **2022**, *14*, 32598–32607. [\[CrossRef\]](#)
2. Esteban, R.; Baumberg, J.J.; Aizpurua, J. Molecular Optomechanics Approach to Surface-Enhanced Raman Scattering. *Acc. Chem. Res.* **2022**, *55*, 1889–1899. [\[CrossRef\]](#) [\[PubMed\]](#)
3. Lv, Q.; Tan, J.; Wang, Z.; Yu, L.; Liu, B.; Lin, J.; Li, J.; Huang, Z.-H.; Kang, F.; Lv, R. Femtomolar-Level Molecular Sensing of Monolayer Tungsten Diselenide Induced by Heteroatom Doping with Long-Term Stability. *Adv. Funct. Mater.* **2022**, *2022*, 2200273. [\[CrossRef\]](#)
4. Zhou, J.; Guo, J.; Mebel, A.M.; Ghimire, G.; Liang, F.; Chang, S.; He, J. Probing the Intermediates of Catalyzed Dehydration Reactions of Primary Amide to Nitrile in Plasmonic Junctions. *ACS Catal.* **2022**, *12*, 7737–7747. [\[CrossRef\]](#)
5. Li, H.; Merkl, P.; Sommertune, J.; Thersleff, T.; Sotiriou, G.A. SERS Hotspot Engineering by Aerosol Self-Assembly of Plasmonic Ag Nanoaggregates with Tunable Interparticle Distance. *Adv. Sci.* **2022**, *2022*, 2201133. [\[CrossRef\]](#)
6. Nguyen, L.B.T.; Leong, Y.X.; Koh, C.S.L.; Leong, S.X.; Boong, S.K.; Sim, H.Y.F.; Phan-Quang, G.C.; Phang, I.Y.; Ling, X.Y. Inducing Ring Complexation for Efficient Capturing and Detection of Small Gaseous Molecules Using SERS for Environmental Surveillance. *Angew. Chem. Int. Ed.* **2022**, *134*, e202207447. [\[CrossRef\]](#)
7. Dong, Y.; Gong, M.; Shah, F.U.; Laaksonen, A.; An, R.; Ji, X. Phosphonium-Based Ionic Liquid Significantly Enhances SERS of Cytochrome c on TiO<sub>2</sub> Nanotube Arrays. *ACS Appl. Mater. Interfaces* **2022**, *14*, 27456–27465. [\[CrossRef\]](#)
8. Wang, W.; Rahman, A.; Huang, Q.; Vikesland, P.J. Surface-Enhanced Raman Spectroscopy Enabled Evaluation of Bacterial Inactivation. *Water Res.* **2022**, *220*, 118668. [\[CrossRef\]](#)
9. Zheng, Z.; Luo, Y.; Yang, H.; Yi, Z.; Zhang, J.; Song, Q.; Yang, W.; Liu, C.; Wu, X.; Wu, P. Thermal Tuning of Terahertz Metamaterial Absorber Properties based on VO<sub>2</sub>. *Phys. Chem. Chem. Phys.* **2022**, *24*, 8846–8853. [\[CrossRef\]](#)
10. Zheng, Z.; Zheng, Y.; Luo, Y.; Yi, Z.; Zhang, J.; Liu, Z.; Yang, W.; Yu, Y.; Wu, X.; Wu, P. A Switchable Terahertz Device Combining Ultra-Wideband Absorption and Ultra-Wideband Complete Reflection. *Phys. Chem. Chem. Phys.* **2022**, *24*, 2527–2533. [\[CrossRef\]](#)
11. Wu, X.; Zheng, Y.; Luo, Y.; Zhang, J.; Yi, Z.; Wu, X.; Cheng, S.; Yang, W.; Yu, Y.; Wu, P. A Four-Band and Polarization-Independent BDS-based Tunable Absorber with High Refractive Index Sensitivity. *Phys. Chem. Chem. Phys.* **2021**, *23*, 26864–26873. [\[CrossRef\]](#) [\[PubMed\]](#)
12. Xiong, J.; Dong, C.; Zhang, J.; Fang, X.; Ni, J.; Gan, H.; Li, J.; Song, C. DNA Walker-Powered Ratiometric SERS Cytosensor of Circulating Tumor Cells with Single-Cell Sensitivity. *Biosens. Bioelectron.* **2022**, *213*, 114442. [\[CrossRef\]](#) [\[PubMed\]](#)
13. Sahoo, S.R.; Hsu, S.H.-J.; Chou, D.-A.; Wang, G.-J.; Chang, C.C. Surface Plasmon-Enhanced Fluorescence and Surface-Enhanced Raman Scattering Dual-Readout Chip Constructed with Silver Nanowires: Label-Free Clinical Detection of Direct-Bilirubin. *Biosens. Bioelectron.* **2022**, *213*, 114440. [\[CrossRef\]](#) [\[PubMed\]](#)
14. Chen, M.; Zhang, J.; Zhu, X.; Liu, Z.; Huang, J.; Jiang, X.; Fu, F.; Lin, Z.; Dong, Y. Hybridizing Silver Nanoparticles in Hydrogel for High-Performance Flexible SERS Chips. *ACS Appl. Mater. Interfaces* **2022**, *14*, 26216–26224. [\[CrossRef\]](#)
15. Man, T.; Lai, W.; Zhu, C.; Shen, X.; Zhang, W.; Bao, Q.; Chen, J.; Wan, Y.; Pei, H.; Li, L. Perovskite Mediated Vibronic Coupling of Semiconducting SERS for Biosensing. *Adv. Funct. Mater.* **2022**, *2022*, 2201799. [\[CrossRef\]](#)
16. Park, S.; Jeon, C.S.; Choi, N.; Moon, J.-I.; Lee, K.M.; Pyun, S.H.; Kang, T.; Choo, J. Sensitive and Reproducible Detection of SARS-CoV-2 using SERS-Based Microdroplet Sensor. *Chem. Eng. J.* **2022**, *446*, 137085. [\[CrossRef\]](#)
17. Nie, M.; Zhao, Y.; Nam, W.; Song, J.; Zhu, W.; Lezec, H.J.; Agrawal, A.; Zhou, W. Broadband Nanoscale Surface-Enhanced Raman Spectroscopy by Multiresonant Nanolaminate Plasmonic Nanocavities on Vertical Nanopillars. *Adv. Funct. Mater.* **2022**, *2022*, 2202231. [\[CrossRef\]](#)
18. Nahi, O.; Broad, A.; Kulak, A.N.; Freeman, H.M.; Zhang, S.; Turner, T.D.; Roach, L.; Darkins, R.; Ford, I.J.; Meldrum, F.C. Positively Charged Additives Facilitate Incorporation in Inorganic Single Crystals. *Chem. Mater.* **2022**, *34*, 4910–4923. [\[CrossRef\]](#)
19. Cai, J.; Wang, Z.; Jia, S.; Feng, Z.; Ren, Y.; Lin, L.; Chen, G.; Zheng, Z. Si/TiO<sub>2</sub>/Ag Multistorey Structures with Interfacial Charge Transfer for a Recyclable Surface-Enhanced Raman Scattering Substrate. *ACS Appl. Mater. Interfaces* **2022**, *14*, 13703–13712. [\[CrossRef\]](#)
20. Tian, Y.; Hu, H.; Chen, P.; Dong, F.; Huang, H.; Xu, L.; Yan, L.; Song, Z.; Xu, T.; Chu, W. Dielectric Walls/Layers Modulated 3D Periodically Structured SERS Chips: Design, Batch Fabrication, and Applications. *Adv. Sci.* **2022**, *9*, 2200647. [\[CrossRef\]](#)
21. Garg, A.; Mejia, E.; Nam, W.; Nie, M.; Wang, W.; Vikesland, P.; Zhou, W. Microporous Multiresonant Plasmonic Meshes by Hierarchical Micro–Nanoimprinting for Bio-Interfaced SERS Imaging and Nonlinear Nano-Optics. *Small* **2022**, *18*, 2106887. [\[CrossRef\]](#) [\[PubMed\]](#)
22. Gu, W.; Zhao, Y.; Zhuang, S.; Zha, J.; Dong, J.; You, Q.; Gan, Z.; Xia, N.; Li, J.; Wu, Z.; et al. Unravelling the Structure of a Medium-Sized Metalloid Gold Nanocluster and its Filming Property. *Angew. Chem. Int. Ed.* **2021**, *60*, 11184–11189. [\[CrossRef\]](#) [\[PubMed\]](#)
23. Huang, J.; Ma, D.; Chen, F.; Chen, D.; Bai, M.; Xu, K.; Zhao, Y. Green in Situ Synthesis of Clean 3D Chestnutlike Ag/WO<sub>3-x</sub> Nanostructures for Highly Efficient, Recyclable and Sensitive SERS Sensing. *ACS Appl. Mater. Interfaces* **2017**, *9*, 7436–7446. [\[CrossRef\]](#) [\[PubMed\]](#)
24. Ma, L.; Wu, H.; Huang, Y.; Zou, S.; Li, J.; Zhang, Z. High-Performance Real-Time SERS Detection with Recyclable Ag Nanorods@HfO<sub>2</sub> Substrates. *ACS Appl. Mater. Interfaces* **2016**, *8*, 27162–27168. [\[CrossRef\]](#) [\[PubMed\]](#)

25. Butmee, P.; Samphao, A.; Tumcharern, G. Reduced Graphene Oxide on Silver Nanoparticle Layers-Decorated Titanium Dioxide Nanotube Arrays as SERS-Based Sensor for Glyphosate Direct Detection in Environmental Water and Soil. *J. Hazard. Mater.* **2022**, *437*, 129344. [\[CrossRef\]](#)
26. Zhou, L.; Zhou, J.; Lai, W.; Yang, X.; Meng, J.; Su, L.; Gu, C.; Jiang, T.; Li, Q.; Han, J.; et al. Irreversible Accumulated SERS Behavior of the Molecule-Linked Silver and Silver-Doped Titanium Dioxide Hybrid System. *Nat. Commun.* **2020**, *11*, 1785. [\[CrossRef\]](#)
27. Chen, C.; Wang, X.; Zhang, Y.; Li, X.; Gao, H.; Waterhouse, G.I.N.; Qiao, X.; Xu, Z. A Molecularly-Imprinted SERS Sensor Based on a TiO<sub>2</sub>@Ag Substrate for the Selective Capture and Sensitive Detection of Tryptamine in Foods. *Food Chem.* **2022**, *394*, 133536. [\[CrossRef\]](#)
28. Mu, W.Q.; Hwang, D.K.; Chang, R.P.H.; Ketterson, J.B. Silver-Coated Inverse Opals Formed from Polystyrene Spheres for Surface-Enhanced Raman Scattering. *J. Raman Spectrosc.* **2011**, *42*, 941–944. [\[CrossRef\]](#)
29. Li, J.Y.; Zhang, S.F.; Yang, J.; Zheng, X.D. Improved SERS Sensitivity of TiO<sub>2</sub> Nanorod Films by Annealing in Vacuum. *Vacuum* **2021**, *194*, 110579. [\[CrossRef\]](#)
30. Li, L.; Dong, J.; Qian, W.P. Research in the Preparation and Application of Nanobowl Arrays. *Prog. Chem.* **2018**, *30*, 156–165.
31. Ai, B.; Wang, Z.; Mohwald, H.; Zhang, G. Plasmonic Nanochemistry Based on Nanohole Array. *ACS Nano* **2017**, *11*, 12094–12102. [\[CrossRef\]](#)
32. Geng, C.; Zheng, L.; Yu, J.; Yan, Q.; Wei, T.; Wang, X.; Shen, D. Thermal Annealing of Colloidal Monolayer at the Air/Water Interface: A Facile Approach to Transferrable Colloidal Masks with Tunable Interstice Size for Nanosphere Lithography. *J. Mater. Chem.* **2012**, *22*, 22678–22685. [\[CrossRef\]](#)
33. Jin, X.; Zhu, Q.; Feng, L.; Li, X.; Zhu, H.; Miao, H.; Zeng, Z.; Wang, Y.; Li, Y.; Wang, L.; et al. Light-Trapping SERS Substrate with Regular Bioinspired Arrays for Detecting Trace Dyes. *ACS Appl. Mater. Interfaces* **2021**, *13*, 11535–11542. [\[CrossRef\]](#) [\[PubMed\]](#)
34. Shi, G.; Lu, N.; Gao, L.; Xu, H.; Yang, B.; Li, Y.; Wu, Y.; Chi, L. Fabrication of TiO<sub>2</sub> Arrays Using Solvent-Assisted Soft Lithography. *Langmuir* **2009**, *25*, 9639–9643. [\[CrossRef\]](#) [\[PubMed\]](#)
35. Kobayashi, Y.; Salgueirino-Maceira, V.; Liz-Marzan, L.M. Deposition of Silver Nanoparticles on Silica Spheres by Pretreatment Steps in Electroless Plating. *Chem. Mater.* **2001**, *13*, 1630–1633. [\[CrossRef\]](#)
36. Zhang, S.F.; Zhao, H.; Li, X.; Li, Y.; Jin, Y.B.; Liu, X.F.; Shi, G.; Wong, P.K. A Hierarchical Si<sub>3</sub>N<sub>4</sub>/CN/MoS<sub>2</sub> Photocathode with Low Internal Resistance and Strong Light-Absorption for Solar Hydrogen Production. *Appl. Catal. B-Environ.* **2022**, *300*, 120758. [\[CrossRef\]](#)
37. Li, X.; Li, Y.; Wang, H.; Miao, H.; Zhu, H.; Liu, X.; Lin, H.; Shi, G. Fabrication of a Three-Dimensional Bionic Si/TiO<sub>2</sub>/MoS<sub>2</sub> Photoelectrode for Efficient Solar Water Splitting. *ACS Appl. Energ. Mater.* **2021**, *4*, 730–736. [\[CrossRef\]](#)
38. Zhang, S.; Chen, J.; Zheng, J.; Chen, X.; Xu, H.; Petrescu, F.I.T.; Ungureanu, L.M.; Shi, G. A Simple Polypyrrole/Polyvinylidene Fluoride Membrane with Hydrophobic and Self-Floating Ability for Solar Water Evaporation. *Nanomaterials* **2022**, *12*, 859. [\[CrossRef\]](#)
39. Wang, Y.; Feng, L.; Zhu, H.; Miao, H.; Li, Y.; Liu, X.; Shi, G. Noncontact Metal–Spiropyran–Metal Nanostructured Substrates with Ag and Au@SiO<sub>2</sub> Nanoparticles Deposited in Nanohole Arrays for Surface-Enhanced Fluorescence and Trace Detection of Metal Ions. *ACS Appl. Nano Mater.* **2021**, *4*, 3780–3789. [\[CrossRef\]](#)
40. Sun, H.; Li, X.; Chen, J.; Zhu, H.; Miao, H.; Li, Y.; Liu, X.; Shi, G. A Novel Photothermal, Self-Healing and Anti-Reflection Water Evaporation Membrane. *Soft Matter* **2021**, *17*, 4730–4737. [\[CrossRef\]](#)
41. Shi, G.; Zhang, X.; Li, J.; Zhu, H.; Li, Y.; Zhang, L.; Ni, C.; Chi, L. Fabrication of 3D Biomimetic Composite Coating with Broadband Antireflection, Superhydrophilicity, and Double p–n Heterojunctions. *Nano Res.* **2017**, *10*, 2377–2385. [\[CrossRef\]](#)
42. Chen, H.; Chen, Z.; Yang, H.; Wen, L.; Yi, Z.; Zhou, Z.; Dai, B.; Zhang, J.; Wu, X.; Wu, P. Multi-mode Surface Plasmon Resonance Absorber based on Dart-Type Single-Layer Graphene. *RSC Adv.* **2022**, *12*, 7821–7829. [\[CrossRef\]](#) [\[PubMed\]](#)
43. Zhao, F.; Lin, J.; Lei, Z.; Yi, Z.; Qin, F.; Zhang, J.; Liu, L.; Wu, X.; Yang, W.; Wu, P. Realization of 18.97% Theoretical Efficiency of 0.9  $\mu$ m Thick c-Si/ZnO Heterojunction Ultrathin-Film Solar Cells via Surface Plasmon Resonance Enhancement. *Phys. Chem. Chem. Phys.* **2022**, *24*, 4871–4880. [\[CrossRef\]](#) [\[PubMed\]](#)
44. Zhou, F.; Qin, F.; Yi, Z.; Yao, W.T.; Liu, Z.; Wu, X.; Wu, P. Ultra-wideband and Wide-Angle Perfect Solar Energy Absorber based on Ti Nanorings Surface Plasmon Resonance. *Phys. Chem. Chem. Phys.* **2021**, *23*, 17041–17048. [\[CrossRef\]](#) [\[PubMed\]](#)
45. Li, Y.; Feng, L.; Li, J.; Li, X.; Chen, J.; Wang, L.; Qi, D.; Liu, X.; Shi, G. Fabrication of an Insect-like Compound-eye SERS Substrate with 3D Ag Nano-bowls and its Application in Optical Sensor. *Sensor. Actuat. B-Chem.* **2021**, *330*, 129357. [\[CrossRef\]](#)
46. Yang, W.; Li, Z.; Lu, Z.; Yu, J.; Huo, Y.; Man, B.; Pan, J.; Si, H.; Jiang, S.; Zhang, C. Graphene-Ag Nanoparticles-Cicada Wings Hybrid System for Obvious SERS Performance and DNA Molecular Detection. *Opt. Express* **2019**, *27*, 3000–3013. [\[CrossRef\]](#)